Supplementary Material: T. Hogan *et al.*, First-order melting of a weak spin-orbit Mott insulator into a correlated metal

Crystal Growth/Characterization

Single crystals were synthesized via a flux growth technique. High purity powders of $SrCO_3$, IrO_2, and La_2O_3 (Alfa Aesar) were dried, and stoichiometric amounts were measured out, employing a 15:1 molar ratio between $SrCl_2$ flux and target composition. Powders were loaded into a platinum crucible and reacted. DI water was used to dissolve the $SrCl_2$ flux and expose the crystals grown at the base of the crucible. Typical crystals had a plate-like habit with dimensions typically of 1 mm x 1 mm x 0.2 mm. Dopant content was determined by energy-dispersive x-ray spectroscopy (EDS) measurements. Crystals were rinsed in DI water to dissolve any remnant flux and cleaved to ensure clean surfaces for measurement. Each sample concentration reported here represents the average of 15-20 individual measurements of randomly sampled 20μm x 20μm areas with the error bars reflecting one standard deviation of this sampling set. Smaller sampling windows were also used to confirm homogeneity across the sample within the 20 μm footprint.

Powder X-Ray Diffraction Measurements

Crystals previously characterized via EDS were ground into a fine powder and measured in either a Bruker D2 Phaser or a PANalytical Empyrean x-ray diffractometer at room temperature. No impurity phases were observed within instrument resolution. Lattice parameters and unit cell volumes were refined within the *Bbcb* orthorhombic space group as shown in Fig. 1 (c). The doping-dependence of the c-axis lattice parameter is presented in Fig. S1. The angular resolution of the instrument and intrinsic broad peak width of c-axis reflections preclude any systematic trend to be discerned (ie. shifts in peak positions small relative to c-axis crystallinity). In order to obtain a global average for samples within a batch, data below 4.5% were binned into 1% wide bins centered at integer concentrations. Error bars for a single measurement of lattice parameter values correspond to the standard deviation output of the PANalytrical HighScore+ software package.

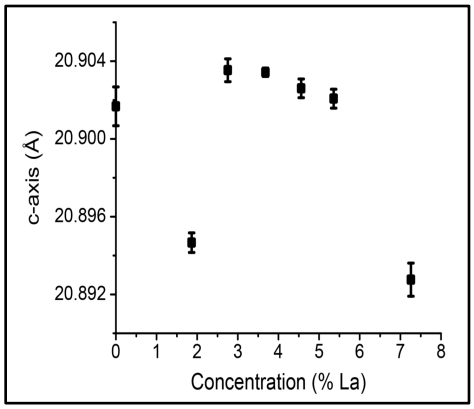

Fig. S1: Room temperature c-axis lattice parameter of $(Sr_{1-x}La_x)_3Ir_2O_7$ as a function La-concentration.

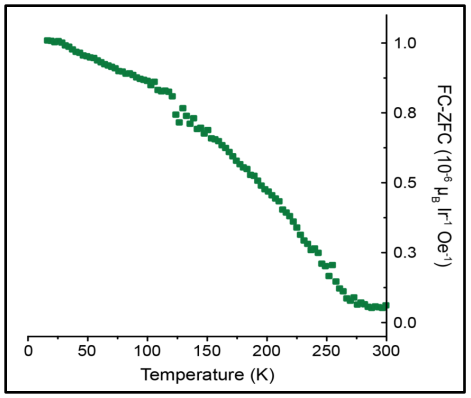

Fig. S2: FC-ZFC susceptibility data for x=0.074 Ca-doped Sr-327. Data was collected under 100 Oe applied parallel to the ab-plane.

Bulk Electronic Properties Measurements

Electronic transport measurements were carried out using a four-probe contact configuration and measured with a Lakeshore 370 AC Resistance Bridge. Measurements were performed in a Janis Research Company CCR with a base temperature of 3K. Magnetization measurements were collected with a Quantum Design MPMS 5XL SQUID magnetometer and MPMS3 SQUID-VSM magnetometer. Heat capacity measurements were

collected within a Quantum Design physical property measurement system (PPMS). The irreversible portion of the static spin susceptibility for $(Sr_{1-x}Ca_x)_3Ir_2O_7$ x=0.074 is shown in Fig. S2. The difference between field cooled and zero field cooled measurements reveals a magnetic phase transition T_{AF}~270K, close to that of the unalloyed parent material.

Neutron Diffraction Experimental Setup:

Elastic neutron scattering experiments were conducted at the N5 beamline at Chalk River Laboratories. Samples were mounted to thin (0.4mm) Al plates with a drop of CYTOP fluoropolymer, cured at 100C for one hour. Sample orientation is known to have the c-axis perpendicular to the face of these small platelets, and the a-axis is often found parallel to a long, regular edge of the sample. Samples were aligned within a closed cycle refrigerator (CCR) in the H0L plane using the approximate *orthorhombic Bbcb* symmetry. Experiments were performed with pyrolytic graphite (PG) monochrometer and analyzer crystals using the Q=(0,0,2) reflection. The incident wavelength was 14.58 meV (2.37051 Å) and collimations of open – 36' – 33' – 144' were used before the monochromator, sample, analyzer, and detector, respectively.

Resonant X-Ray Diffraction Experimental Setup:

Resonant elastic x-ray diffraction experiments were carried out at the 6-ID-B beamline at the Advanced Photon Source at Argonne National Laboratory and the X22C beamline at the National Synchrotron Light Source at Brookhaven National Laboratory. The radiation source was an undulator insertion device at 6-ID-B and a bending magnet at X22C. Samples were mounted using a small spot of GE varnish to a small copper mount. This mount was connected to the cold head of a CCR using Be domes for the radiation shield and vacuum shroud. Samples were aligned in the H0L plane on [0 0 20] and [2 0 10] Bragg reflections indexed to the orthorhombic Bbcb space group. Data was collected with incident energy tuned to the resonant peak corresponding to the Ir L_3 edge (11.22 keV). Experiments on X22C utilized a Si(111) analyzer. 6-ID-B utilized a PG-008 crystal for polarization analysis.

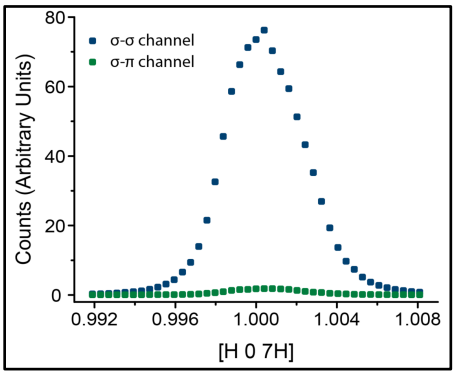

Fig. S3: Radial scans through the (1,0,7) reflection in both σ-σ and σ-π scattering channels for La-doped Sr-327 x=0.058. Data from 6-ID-B

Measurements collected on 6-ID-B showed that the superlattice observed at **Q**=(odd, 0, odd) positions was nonmagnetic in origin. Representative data are shown in Fig. S3 Data from a x=0.058 $(Sr_{1-x}La_x)_3Ir_2O_7$ sample at 6K, which shows scattering in σ-σ and σ-π channels for the [1 0 7] reflection. The σ-π peak intensity is ~ 2.4% that of σ-σ peak and simply arises from bleed through from the σ-σ scattering channel.

Resonant X-ray measured order parameters:

Resonant elastic x-ray scattering measurements at 11.22 keV were utilized to determine select transition temperatures in Fig. 4 of the main manuscript. These transition temperatures were derived from order parameter measurements shown in the Figs. S4-S6 below:

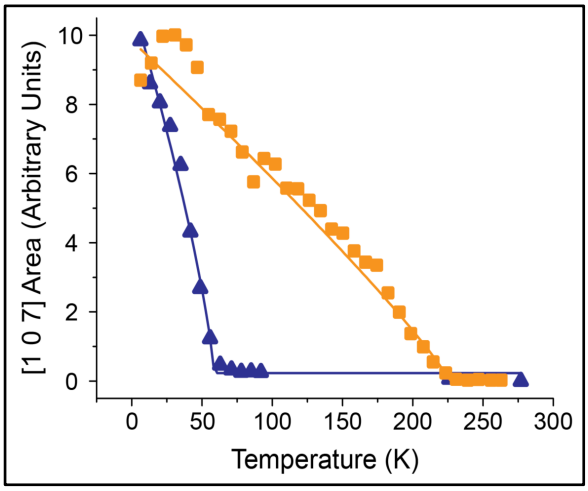

Fig. S4: Q=(1,0,7) integrated intensity as a function of temperature, determining T_S for x=0.058 (yellow squares) and x=0.023 (blue triangles. Data is from 6-ID-B collected in σ–σ

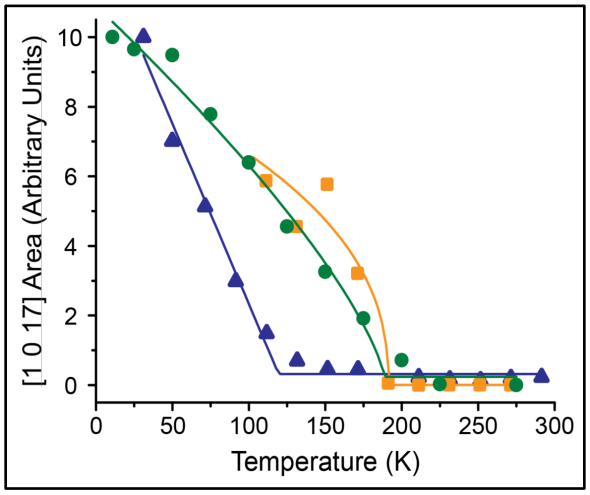

Fig. S5: Q=(1,0,17) integrated intensity as a function of temperature determining T_S for x=0.046 (yellow squares), x=0.53 (green circles), and x=0.027 (blue triangles). Data is from X22C.

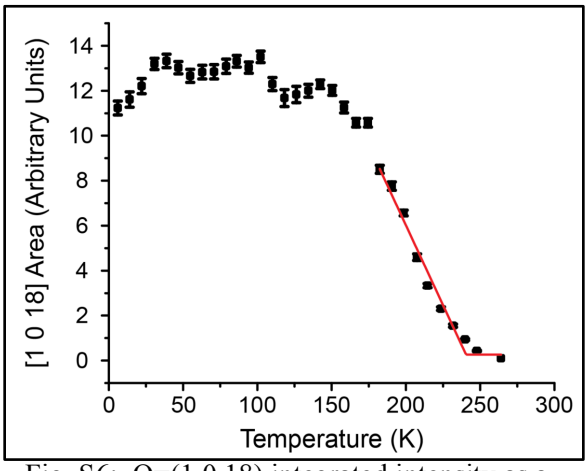

Fig. S6: Q=(1,0,18) integrated intensity as a function of temperature determining T_{AF} for x=0.023. Data is from 6-ID-B collected in σ-π.

Scanning Tunneling Microscopy/Spectroscopy Experimental Setup:

Scanning tunneling microscopy/spectroscopy (STM/S) measurements were performed at 4K using etched W tips, on samples cleaved at ~77K in UHV. Cleavage occurs between SrO layers and, consistent with earlier reports [1], the atoms imaged in STM topographies belong to the Sr sublattice of the exposed SrO plane. dI/dV spectra were taken by the usual Lock-in technique, with tip height fixed in constant-current mode at +330 mV and -300 mV for maps shown in the main text Figs. 3(c) and (d) respectively. Individual La dopants appear as squares in the topography (Fig. 3 (a) and (b)). In electronically phase-separated samples density fluctuations of La-dopants were not strongly correlated with the metal/insulator nature of the dI/dV spectra (ie. the chemical location of La-dopants was not correlated with the location of metallic puddles). The evolution of this effect and the role of surface and subsurface La dopants in destroying the insulating state locally will be discussed elsewhere [2].

Combined analysis of static spin susceptibility and STS spectroscopy to exclude rare moment clusters with a charge gap:

The Curie-Weiss behavior observed in x=0.058 La-doped Sr-327 can be shown to originate from metallic (electronically gapless) regions of the sample, and not from rare-region spin clusters with a spectral gap, via a comparison of the static spin susceptibility data with STS spectroscopy. Below we outline how these two scenarios can be discriminated.

We can first consider what the volume fraction of the hypothetical clustered local moments within the sample should be in order to attain the effective Curie-Weiss (CW) observed in Fig. 2 (d) of the main manuscript. The parent $Sr_3Ir_2O_7$ material does not show high-temperature CW behavior due to the persistence of robust short-range AF correlations above T_N~280K [3]. So in assuming what the local moments of Ir-ions in the clusters could be, we will consider the strictest scenario by using the full S=1/2 local moment $\mu_{local} = 1.73\ \mu_B$ as the nominal Ir local moment. This local impurity moment can only generate the observed/apparent CW behavior of 0.51 m_B/Ir site if full 1.73 μ_B moments occupied ~9% of the sample volume.

To exclude this possibility: The STM data in the main manuscript Figure 3 (b) show a 15 nm x 15 nm topographic map of the sample, whose spectral histogram is plotted in Fig. 3 (d). Within this map, no gapped regions were observed. This corresponds to a 22,500 $Å^2$ area map and a survey of 1480 unit cells (with a=b=3.897 Å). The tetragonal unit cell has 3.897 Å as the nearest neighbor Ir-Ir distance, and there is one Ir-cation per 3.897 Å × 3.897 Å square. The positional binning of the spectral histogram is 2.4 Å × 2.4 Å. Our observation of no gapped regions within the STS spectra therefore means that the upper limit for the volume fraction of gapped regions (presumably with clustered magnetic moments) is 0.07%. This is two orders of magnitude smaller than what is necessary to account for the local moment cluster explanation of susceptibility data. Hence, rare, gapped regions with local moments cannot account for the observed susceptibility.

Similarly we can consider a second scenario where clusters of ferromagnetic spins saturate under the applied H-field and, via disorder, mimic a CW response. If we again assume the strictest case where full moments of 1 μ_B/Ir occupy the polarized clusters, we can then ask what volume fraction of the sample would be needed to host these polarized clusters (again presumably with an accompanying spectral gap). The measured χ(T) and applied field given in Fig. 2 (d) give a lower limit on the volume fraction of such

clustered regions of 0.36% of the sample volume. This worst-case estimate is precluded by the gapless sample volume fraction surveyed in Fig. 3(b) and (d) as detailed above. Additionally, larger STS maps surveying 562,500 $Å^2$ were also collected and spectral histograms analyzed on this same sample [2]. These also revealed no gapped spectra, which further reduces the possible volume fraction of gapped regions to be smaller than 0.003% of the sample volume. As a result, the combined data necessitates moments coexisting with the metallic state in this sample.

[1] Y. Okada et al. Nature Materials 12, 707–713 (2013)
[2] D. Walkup et al., in preparation.
[3] I. Nagai et al., Journal of Physics: Condensed Matter 19, 136214 (2007).